RSC Advances

ROYAL SOCIETY OF CHEMISTRY

www.rsc.org/advances

Journal Name

RSCPublishing

ARTICLE

Charged particle-induced synthesis of carbon nanowalls and characterization

Cite this: DOI: 10.1039/x0xx00000x

Takashi Uchida*[a,b], Ankur Baliyan†[b], Takahiro Fukuda[b], Yoshikata Nakajima[a,b], Yoshikazu Yoshida[b,c]

Received 00th January 2012,
Accepted 00th January 2012

DOI: 10.1039/x0xx00000x

www.rsc.org/

We demonstrate growth and characterization of carbon nanowall (CNW) films on silicon substrates by the surface-wave microwave plasma-enhanced chemical vapor deposition method. The grown CNWs in the film show orientation anisotropy. A CNW is composed of well-crystallized nanographite. The deposition of CNW films, in particular the film thickness and nanographite domain size, strongly depends on the carbon feedstock concentration, deposition pressure, distance between substrate and plasma, and deposition duration. The deposition rate of CNWs in terms of CNW film thickness is approximately 1 μm/min. We propose a charged particle-induced growth mechanism of the CNW film, which also follows the thermodynamic nucleation model. Nitrogen gas sorption measurements show that the CNW films have approximately 100 m^2/g Brunauer-Emmett-Teller specific surface area and micro-mesopores.

1. Introduction

Graphite-based nanostructures (GBNs) such as graphene and carbon nanotubes are attracting much attention as a building block for nanotechnology since the GBNs have excellent physical and chemical properties [1, 2]. The synthesis of carbon nanowalls (CNWs), one of the GBNs, was reported by Wu et al. [3]. CNWs are usually obtained on a flat substrate, and have a petal-like morphology, which stands perpendicular to the substrate surface. A typical CNW is a sheet composed of multiple nanographite domains with a length and height of several μm, whereas its thickness is several tens of nm [4]. The peculiar structure of CNWs have several advantages over the other GNBs that makes it more attractive for possible applications of CNWs such as a field emitter, electrode, storage, coating, and so on [5]. Recent results also indicate that CNWs incorporated hybrid materials, significantly, improved the performance of devices in a wide range of applications such as a negative electrode for lithium ion secondary battery [6], super-hydrophobic surface coating [7], thermal insulator [8], and platinum catalyst support for fuel cells [9].

CNWs have been synthesized by various chemical vapor deposition (CVD) techniques, such as a microwave plasma-enhanced CVD (MPECVD) [3, 10-14], radio frequency PECVD [15-18], direct current PECVD [19], electron beam excited PECVD [20], helicon PECVD [21], and hot-filament CVD [22]. Variation in the plasma parameters and electric field distribution of the microwave helped to control over the architectural morphology and the alignment of CNWs [16, 20]. PECVD synthesis of CNWs, that is, vertically oriented graphene nanosheets is very well summarized in elsewhere [23]. However, the control of domain size and edge structure of CNWs has not been successfully achieved yet.

In this study, we grew CNW films by the surface-wave MPECVD (SWMPECVD) method. The grown CNWs are characterized by scanning electron microscopy (SEM), transmission electron microscopy (TEM), X-ray photoelectron spectroscopy (XPS), X-ray diffractometry (XRD), and Raman spectroscopy. We investigated dependences of a thickness and Raman features of CNW films on deposition conditions, such as a carbon feedstock concentration, chamber pressure, distance between the substrate and quartz disk, and deposition duration. Additionally, we propose a charged particle-induced growth mechanism of CNW film. Also, we show nitrogen gas sorption measurement results.

2. Experimental details

2.1 SWMPECVD system

A schematic illustration of the SWMPECVD system used in the present work is shown in Fig. 1. The SWMPECVD system is composed of a plasma source, deposition chamber, gas supply system, and evacuation system, and was developed in collaborating with ULVAC, Inc. The base system is a conventional MPECVD system (CN-CVD-200, ULVAC, Inc.). We modified the plasma source i.e. we use a coaxial-type open-ended dielectric cavity as the plasma source. 2.45 GHz microwave is introduced from the aperture. Due to the size of the aperture, an electric field of the microwave exponentially decreases from the disk surface toward the substrate. Therefore, this plasma source can produce high-density planer plasma. The detail of the plasma source is described elsewhere [24]. A substrate holder, equipped with a halogen lamp heater, is placed

below the plasma source. The distance between the quartz disk and the substrate (D_{sq}) can be varied from 40 mm to 120 mm.

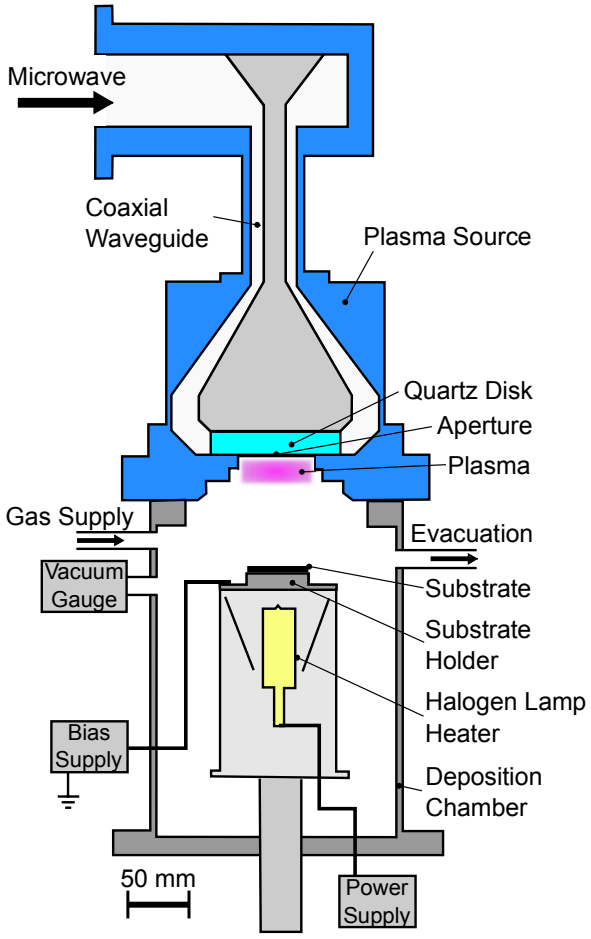

Figure 1. Schematic illustration of the SWMPECVD system using a coaxial-type open-ended dielectric cavity.

The substrate can be applied a positive/negative dc bias voltage. The deposition chamber is evacuated using a rotary pump (400 l/min). The chamber pressure is monitored using a capacitance diaphragm gauge. The process gases are methane (CH_4), hydrogen (H_2), nitrogen (N_2), and oxygen (O_2). We can control the flow rate of each gas using a mass flow controller.

2.2 Deposition of CNW films

CNW films were synthesized on substrates using the following procedure. An n-type low-resistance silicon wafer (ϕ 2 inch-Si (100), mirror-polished, resistivity ≤ 10 Ωcm) was mounted on the substrate holder. The silicon substrate was grounded, i.e. no bias voltage was applied. D_{sq} was set at a certain distance. The deposition chamber was evacuated down to 1 Pascal (Pa). The hydrogen gas was supplied in the chamber with the constant flow rate at 45 standard cubic centimeters per minute (sccm). The chamber pressure (P) was set at a certain pressure. Then the hydrogen plasma was ignited by feeding the microwave (2.45 GHz) power at 350 W. The microwave propagation was tuned using a three-stab-tuner. During the tuning, the substrate heating was started with the heating rate of 100 °C/min. After heating up the substrate to the desired temperature, CH_4 gas was supplied together with H_2 gas at a certain CH_4 gas concentration. The total flow rate of CH_4 gas and H_2 gas was constant at 45 sccm. As the CH_4 gas supply started, the deposition of CNW film started. In order to stop the deposition of CNW film, the microwave feeding, gas supply, and substrate heating were stopped. Finally, system was cooled down to room temperature under nitrogen atmosphere. The substrate temperature (T) was calibrated using a tungsten substrate, to which a thermocouple is attached, for each deposition condition. In the present work, the quartz disk and the substrate (D_{sq}) was varied; 40, 50, and 70 mm. The deposition chamber pressure (P) was varied; 15, 18, 20, 30, and 50 Pa. The concentration of CH_4 gas (C) was varied; 10, 33, 44, and 50 %. The substrate temperature (T) was varied; 540, 605, 660, and 725 °C. The deposition duration (D) was varied; 1, 5, 10, and 15 min.

2.3 Characterization

The surface morphologies of the deposited materials were studied using a scanning electron microscope (JSM-7400F, JEOL Ltd.), and the structures of the deposited materials were analyzed by a transmission electron microscope (JEM-2200FS, JEOL Ltd.). The purity, structural and chemical state of the deposited materials were ascertained by an XPS system (Axis-HSi, Kratos Analytical Ltd.), X-ray diffractometer (SmartLab, Rigaku Corporation), and micro-Raman measurement system (LabRAM HR-800UV, Horiba Jobin Ybon S.A.S.). The physical sorption property was analyzed by a gas sorption measurement system (Autosorb iQ-MP, Quantachrome Instruments). In the XPS measurement, a monochromatized Al Kα X-ray source (1486.6 eV), and were taken at pass energy of 40 eV with 0.1 eV energy steps. The take-off angle of the photoelectrons was maintained at 90° with respect to the surface of samples. In the XRD measurement, Cu Kα line with a wavelength of 0.154 nm was used. We performed in-plane and out-of-plane scans, in which X-ray incidence and detected reflection are, respectively, in and out of the substrate surface. In the Raman measurement, the spectral excitation was provided with a He-Ne laser (633 nm-wavelength) using 100x microscope objective. The laser spot diameter was approx. 1 μm. The excitation laser was incident from the side of the CNW film in order to incident normal to the basal plane of nanographite domains in a CNW sheet.

The plasma was characterized by optical emission spectroscopy (OES). The spectrometer (HR-4000, Ocean optics) combined with an optical fibber (core diameter: 600 μm) was utilized to record the plasma spectra. The tip of the optical fiber was attached to the substrate holder in order to observe the plasma from the below. The position of the substrate holder set to be the farthest in the present system (D_{sq} = 120 mm), so that the entire plasma can be investigated.

3. Results and discussion

Figure 2 (a) and (b) show the top-view and side-view SEM images of as grown material on a silicon substrate. SEM images show that the deposited material on a silicon substrate has uniform morphology similar to that of CNW films in previous reports [3, 13, 15-17, 19-21]. The CNWs stand vertically to the substrate and also form an interconnected network in horizontal direction. The formation of the interconnected network in horizontal direction is unusual and, possibly, might be due to the absence of the substrate bias voltage. In a typical CNW

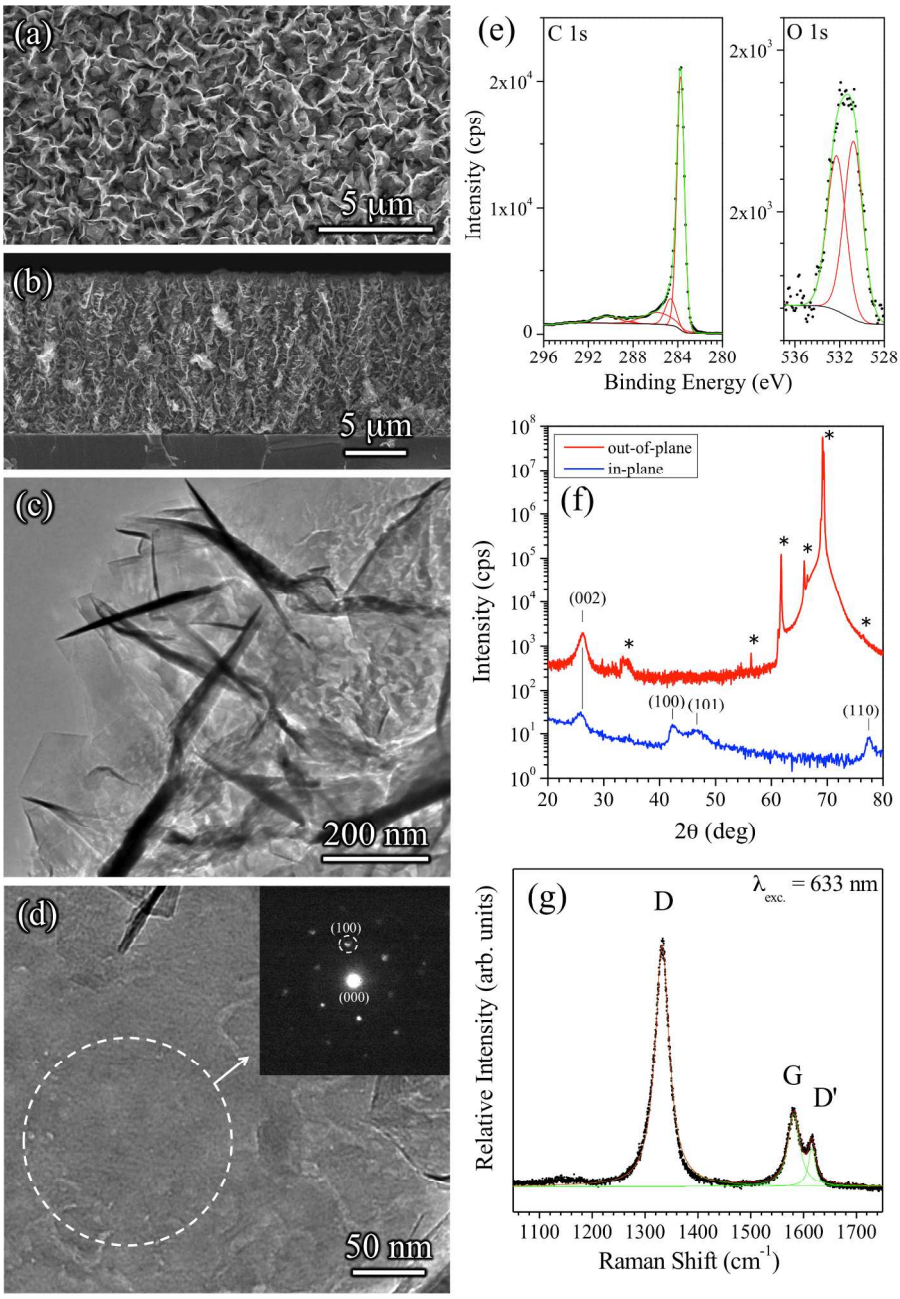

Figure 2. Typical characterization results of grown CNWs by SEM, TEM, XPS, XRD, and Raman spectroscopy. The deposition conditions of the CNW film were; T = 660 °C, P = 20 Pa, C = 33 %, D_{sq} = 40 mm, and D = 15 min. (a) Top-view (b) side-view SEM images of the CNW film on a silicon substrate, (c) low-magnification TEM image of a CNW sheet, (d) high-magnification TEM image and electron diffraction pattern of the CNW sheet, (e) C 1s and O 1s peaks in narrow-scan XPS spectra of the CNW film, (f) XRD profiles of the CNW film with in-plane and out-of-plane scans, and (g) Raman spectrum of the CNW film. The electron diffraction pattern was obtained from a selected area shown as a dotted circle in (d). The XRD peak with an asterisk is originated with the silicon substrate and instrument.

Table 1. Content of oxygen, and carbon obtained by the quantitative analysis of O 1s, and C 1s peak intensities in the XPS spectra. Also the content of sp^2, sp^3 carbons, C-O bonding, carboxylate group obtained by the quantitative analysis of the C 1s peak component intensities are shown.

O (at%)	C (at%)	C 1s (at%)			
		sp^2	sp^3	C-O	O-C=O
3.5	96.5	74	11	14	1

growth, although the CNW film has a smooth surface morphology across the entire substrate, nevertheless, the thickness of the CNW film gradually vary towards the center of the substrate. For 10 minute-deposition period, the thickness at the center and edge of the substrate were found to be approx. 9 and 6 μm, respectively. The detail of the thickness evolution is being discussed in the following section. The weight of the CNW film is approx. 2 mg. Assuming that the average thickness of the film is 7 μm, the volume density of the CNW film is calculated to be approx. 150 kg/m^3, that is much less than that of standard graphite (approx. 2300 kg/m^3).

We analyzed TEM images of individual CNWs. CNWs were scraped off from the silicon substrate and well-dispersed in ethanol before casting them on a TEM micro-grid. Figure 2 (c) shows the low-magnification TEM image of a CNW. There are a lot of foldings and bends across the sheet of the CNW. The edges of the CNW sheet are thinner than the center of that. The high-magnification TEM image as shown in Fig. 2 (d) shows that the planar sheet of the CNW is composed of nanographite domains. The selected area electron diffraction pattern of the CNW at the edge depicts six-fold symmetry. The innermost diffraction spots could be assigned to graphite (100) diffraction spots. The orientation of the diffraction spots was different from place to place in a CNW. Also, two overlapped diffraction patterns were observed, with one six-fold pattern slightly rotated with respect to the other. These results indicate that the CNW sheet is composed of nanographite domains [4].

We performed XPS measurements in order to ascertain the elemental composition, and chemical bonding states of the grown CNW film. Wide-scan XPS spectrum of the CNW film showed only two peaks, which were originated from carbon and oxygen. The C 1s and O 1s peaks in narrow-scan XPS spectra of the CNW film are shown in Fig. 2 (e). A quantitative analysis of the C 1s and O 1s peak intensities reveals that CNW film contains 3.5 at% oxygen atoms as shown in Table 1. The C 1s peak was fitted with five individual mixed Gaussian-Lorentzian curves after a Shirley background subtraction. The main peak at 283.8 eV can be attributed to sp^2 carbon, which is slightly shifted by the typical value (284.5 eV) due to charge-up. Other peaks at 284.6 eV, 285.7 eV, 287.9 eV, and 290.2 eV can be attributed to sp^3 carbon, C-O bonding, carboxylate group (-O–C=O bonding), and π-π* transition loss, respectively. A quantitative analysis of the C 1s peak component intensities are summarized in Table 1. From these spectral features, a CNW is considered to mainly be composed of graphitic structure (sp^2 carbon with π-π stacking). A small amount of sp^3 carbon is supposed to be localized at the "in-wall-boundary" regions [26]. A tiny amount of oxygen is not only physically adsorbed on the CNWs but also chemically bonded to the CNWs. This is also supported by the curve fitting result of the O 1s peak as shown in Fig. 2 (e). The O 1s peak was fitted with two components at 530.7 eV and 532.3 eV. They are respectively originated from physically adsorbed oxygen and C-O bonded oxygen. The chemically bonded oxygen, which is mainly C-O bonding, is also supposed to be localized at the "in-wall-boundary" regions. Figure 2 (f) shows the in-plane and out-of-plane XRD profiles of the CNW film on a silicon substrate. In the out-of-plane XRD profile, graphite (002) reflection peak was observed along with other peaks from the silicon substrate and instrument. In the in-plane XRD profile, graphite (002), (100), (101), and (110) reflection peaks were observed. These XRD profiles reveal that the CNW film is composed of graphitic structure. The graphitic structure in the CNW film is aligned both parallel and vertical with the substrate. The XRD profiles of the CNW film with shorter deposition duration, i.e. the early stage of the CNW film deposition, did not show the graphite (002) reflection peak in in-plane scan but in out-of-plane scan. As revealed in TEM images, graphite *c*-axis is normal to the CNW plane; in other words, basal plane of nanographite domains is parallel to the CNW plane. Therefore, the orientation of CNW in the film is parallel to the substrate surface at the early deposition stage and then change into vertical as the deposition proceeds. This is supported by the previous report [27]. The (002) reflection peak was centered at 25.8° with a full width at half maximum (FWHM) of 1.74°. The interlayer spacing (d_{002}) and domain size along c-axis (L_c) were calculated to be 0.345 nm and 4.9 nm, respectively, using Bragg's law and Scherrer's equation. The number of graphitic layers in a domain is calculated to be approx. 14. Also in-plane domain size (L_a) was calculated from XRD (100), (110) reflection peaks. The L_a

Table 2. Summary of the peak components in the in-plane XRD profile and I_D/I_G from the Raman spectrum. The domain sizes are also summarized. For the domain size estimation, we used Scherrer's equation in the XRD data and an equation in the literature [25] in the Raman data. The domain size along *c*-axis (L_c) was obtained from the XRD (002) reflection peak. The in-plane domain size (L_a) was obtained from the XRD (100), (110) reflection peaks and from the Raman I_D/I_G.

XRD (002)			XRD (100)			XRD (110)			Raman I_D/I_G	
FWHM [deg]	2θ [deg]	L_c [nm]	FWHM [deg]	2θ [deg]	L_a [nm]	FWHM [deg]	2θ [deg]	L_a [nm]	I_D/I_G	L_a [nm]
1.74	25.8	4.9	1.08	42.5	8.2	1.54	77.62	6.9	3.7	10.3

values from (100) and (110) are 8.2 and 6.9 nm, respectively.

Figure 2 (g) shows the Raman spectra of as grown CNW film. In the Raman spectrum, sharp D and G bands are observed at 1329 cm^{-1} and 1579 cm^{-1}, respectively. Also, the D' band at 1615 cm^{-1} can be clearly observed. The widths of the D and G bands are 37 cm^{-1} and 22 cm^{-1}, respectively. The widths of these two Raman bands are very narrow. The D band width indicates the size distribution of the crystallites of nanographitic systems [25]. The G band width (W_G) indicates the degree of graphitization of the domains in CNWs [19]. Therefore, the narrow bandwidths of D and G bands reflect the narrow distribution of the size and the high degree of graphitization of the domains in CNWs. The integrated intensity ratio of the D band to the G band (I_D/I_G) is 3.7. The L_a from the Raman I_D/I_G was estimated to be 10.3 nm, using the equation $L_a = 560/E_{laser}^4(I_D/I_G)^{-1}$ [25], where E_{laser} is the excitation energy in electron volts. The domain size along *c*-axis (L_c) and in-plane domain size (L_a), estimated by the in-plane XRD profile and Raman spectrum, were summarized in Table 2. The characterization results shown in Fig. 2 reveal that the CNW film on the silicon substrate composed of oriented CNWs. The orientation of CNWs proximity to the substrate surface was horizontal and that at the top of the film is vertical. A CNW is composed of well-crystallized nanographite with a lateral and longitudinal dimension of approx. 10 and 5 nm, respectively.

We investigated the effect of *C* on the grown CNWs. CNW films grew, successfully, on silicon substrates with the *C* ranged from 10 to 50 %. Figure 3 shows the *C* dependences with respect to the thickness, I_D/I_G, and W_G of CNW films obtained at T = 660 °C, P = 20 Pa, D_{sq} = 40 mm, and D = 10 min. The thickness at *C* 10 % and 33 % were approx. 3 μm and 9 μm, respectively. The thickness of the CNW film increased with an increase of the *C* from 10 % to 33 %. At higher *C* condition, cf. 40 % and 50 %, the thickness decreased with an

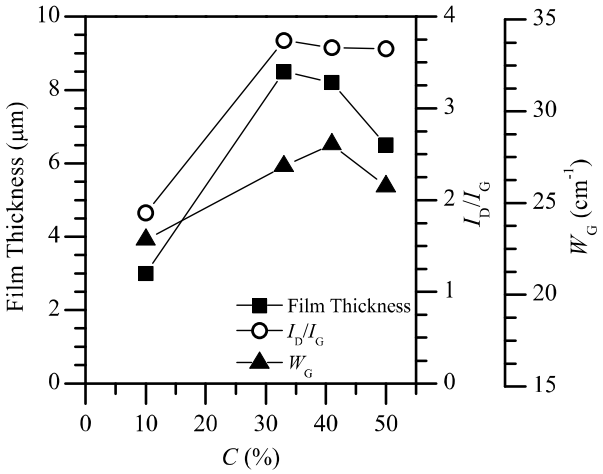

Figure 3. *C* dependences of the thickness, I_D/I_G, and W_G of CNW films obtained with T = 660 °C, P = 20 Pa, D_{sq} = 40 mm, and D = 10 min. The filled squares, open circles, and filled triangles show the film thickness, I_D/I_G, and W_G, respectively. The thickness was analyzed by the side-view SEM image obtained at the center of the substrate.

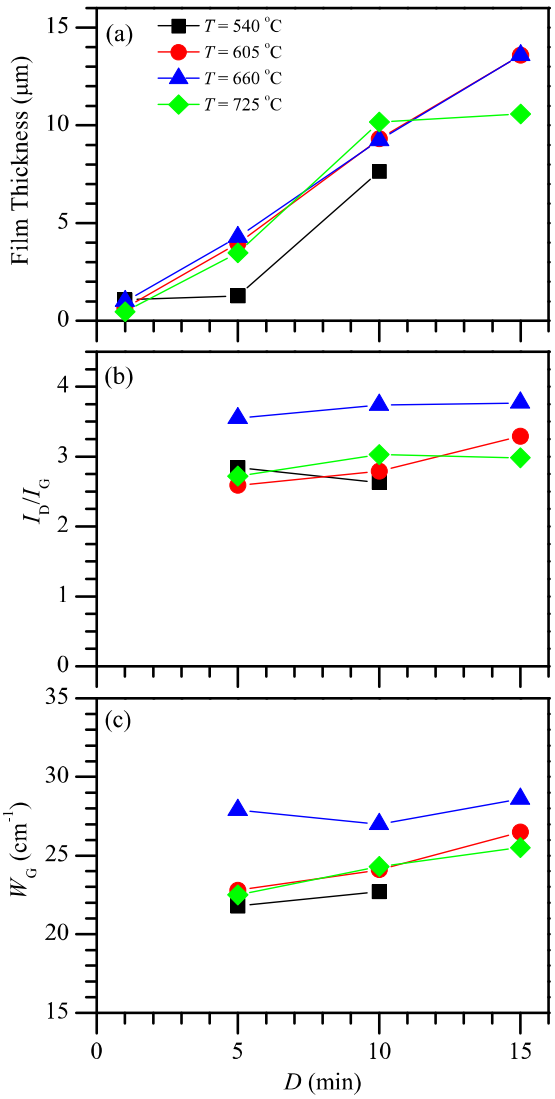

Figure 4. *D* dependences of the thickness, I_D/I_G, and W_G of CNW films obtained with T = 540, 605, 660, 725 °C, P = 20 Pa, C = 33 %, and D_{sq} = 40 mm. The thickness was analyzed by the side-view SEM image obtained at the center of the substrate.

increase of the *C*. At *C* 40 and 50 %, the plasma was hard to maintain, since the quartz disk was covered by carbonous deposit. The I_D/I_G and W_G were almost constant except at *C* 10 %. The L_a from the Raman I_D/I_G was 20.3 and 10.3 nm, respectively, for *C* 10 % and 33 %. The changes in the thickness and the domain size indicate that the number density of nanographite domains was higher at *C* 33 % than that at *C* 10 %. We found the possibility to control the morphology and structure of CNW sheet by changing the *C*. We also investigated the effect of chamber pressure on the grown CNWs. We examined several chamber pressures while keeping the other parameters constant; 15, 18, 20, 30, and 50 Pa (T = 660 °C, C = 33 %, D_{sq} = 40 mm, and D = 10 min.). At less than P 20 Pa, the plasma was too unstable for the deposition and hardly any CNW film could be observed. However, at higher

chamber pressure than 20 Pa, the plasma was stable and a smooth CNW film was found. The thickness of CNW film depended on the chamber pressure. At P 20 Pa, as shown in Fig. 2 (b), the thickness of the CNW film is 9 µm. At P 30 and 50 Pa, the thickness of CNW film was reduced to 10 % as that of P 20 Pa.

We also investigated the effect of D_{sq} on the grown CNWs. The CNW film thickness strongly depends on the D_{sq}. The film thickness decreased with an increase of the D_{sq}. The maximum thickness was obtained at D_{sq} = 40 mm, the minimum distance in the present setup. The thickness of the CNW film at D_{sq} = 40 mm is 9 µm. Then the thickness decreased by a factor of ten at D_{sq} = 50 mm. The CNWs deposition was hardly obtained at D_{sq} = 70mm.

We investigated the effect of substrate temperature and deposition duration on the grown CNW films. The examined substrate temperatures were 540, 605, 660, and 725 °C. The examined deposition durations were 1, 5, 10, and 15 min. Irrespective of the substrate temperature, CNW films grew successfully on silicon substrates. Dependences of the thickness, I_D/I_G, and W_G of CNW films on D obtained at T = 540, 605, 660, 725 °C are shown in Fig. 4. The thickness of CNW film proportionally increased with an increase of the deposition duration regardless of the substrate temperature. The deposition rate of the CNW film thickness is estimated to be 1 µm/min. W_G and I_D/I_G almost unchanged in this substrate temperature and deposition duration ranges. The growth mechanism of CNWs is so complex that they have not yet been fully understood. Let us consider the growth mechanism of the CNW films based on the characterization of the CNW films and plasma. Fig. 5 shows the OES spectrum of the plasma generated under a typical condition in the present study. This spectrum is dominated by the emissions of excited states of H, H_2, CH, and C_2. The intensity of emission of H species is much higher than the other species, since the flow rate of hydrogen is twice as that of methane. C_2 radicals are important for the deposition of graphite materials [28, 29]. The presence of the C_2 peak in the OES spectrum can be seen in Fig. 5. This might take part in the growth of CNWs. However, the exact position, where the observed species in the OES spectrum were generated and disappeared, is unknown. We also checked the electric current, originated with the plasma, to the substrate holder. The current to the holder strongly depends on P and D_{sq}. We observed the ion and electron currents by applying, respectively, negative and positive bias voltages (± 50 V) to the substrate holder. Both the ion and electron currents decrease with an increase of the P and also D_{sq}. At the P greater than 30 Pa, both the ion and electron currents were hardly observed. Also, when D_{sq} is greater than 50 mm, both the ion and electron currents were found to be absent, and hardly any CNWs grew. In this particular study, we did not apply any bias voltage to the substrate during the CNW film deposition. Therefore, both the ions and electrons can reach the substrate and they are supposed to play an important role in the growth of CNWs, that is, they help the formation of the nuclei of nanographite crystallites in CNWs. Ion-induced heterogeneous nucleation, which is

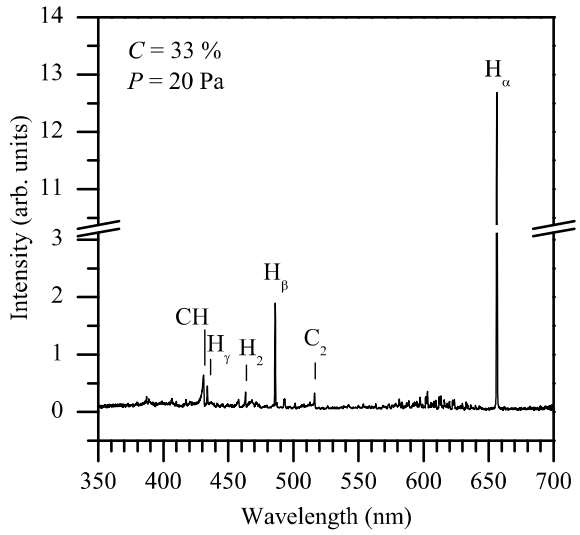

Figure 5. OES spectrum of the plasma generated under typical conditions; P = 20 Pa, C = 33 %, and the microwave power of 350 W.

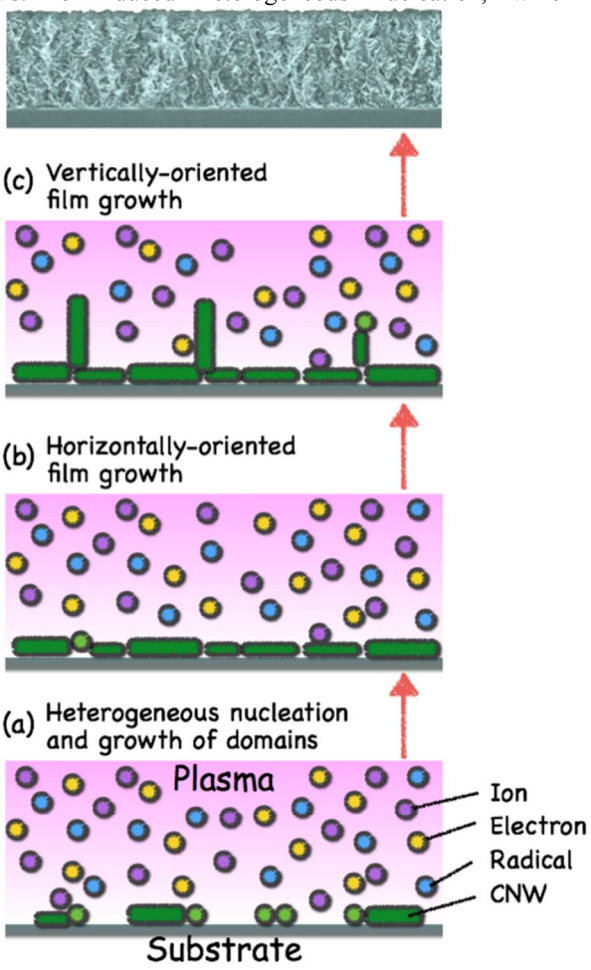

Figure 6. Growth model of CNWs: (1) energetic charged particle (ion and electron)-induced heterogeneous nucleation and growth of domains, (2) horizontally-oriented CNW film growth, and (3) vertically-aligned CNW film growth.

proposed by Thomson[30], is actually common in the growth of diamond[31, 32]. Based on these results, the growth of CNWs follows the Thomson's energetic charged particle-induced heterogeneous nucleation model and can also be described as continuous processes of nucleation and growth of nanographite crystallites. The crystallites form oriented CNWs as shown in Fig. 6. In addition, the growth rate of the CNW film and the domain size (L_a) of CNWs are affected by the carbon concentration (C). The experimental results showed that the CNWs with a greater film thickness and smaller domain size were obtained at higher carbon concentration (C 33%): the less number large size domains are grown at lower carbon concentration (C 10 %). In the thermodynamic model of the nucleation, the supersaturation ratio (S) is important parameter in order to consider the critical nucleus size (R^*), nucleation rate (J), and free energy of the critical nucleus (ΔG^*); $R^* \sim 1/(k_B T \ln S)^3$; $J \sim$□□□□□□)$^{1/2}$ exp($-\Delta G^*/k_B T$); $\Delta G^* \sim$□□^{2}, where k_B is the Boltzmann constant, and T is temperature in kelvins. In this particular case, carbon concentration can be equivalent to the supersaturation ratio. If the carbon concentration is increased, the size is decreased but the number is increased. Therefore, the experimental results are consistent qualitatively with the thermodynamic model.

We observed the nitrogen adsorption-desorption property of the CNWs. Figure 7 shows the nitrogen adsorption-desorption isotherm of the CNWs, which is obtained in the following growth conditions: T = 660 °C, C = 33 %, D_{sq} = 40 mm, and D = 10 min. The isotherm can be assigned as type II in the International Union of Pure and Applied Chemistry (IUPAC) classification scheme. The specific surface area was calculated to be 96.2 m^2/g from the adsorption data in the relative pressure range of 0.05 – 0.3 using the 11 points Brunauer-Emmett-Teller (BET) method. We performed micropore analysis using the quenched solid density functional theory (QSDFT) kernel [33], assuming slit pore geometry. The pores in CNWs show micro-mesopore size distribution with peaks at 0.7 nm and 2.6 nm as shown in the inset of Fig. 7. The pore volume is approx. 0.2 cc/g.

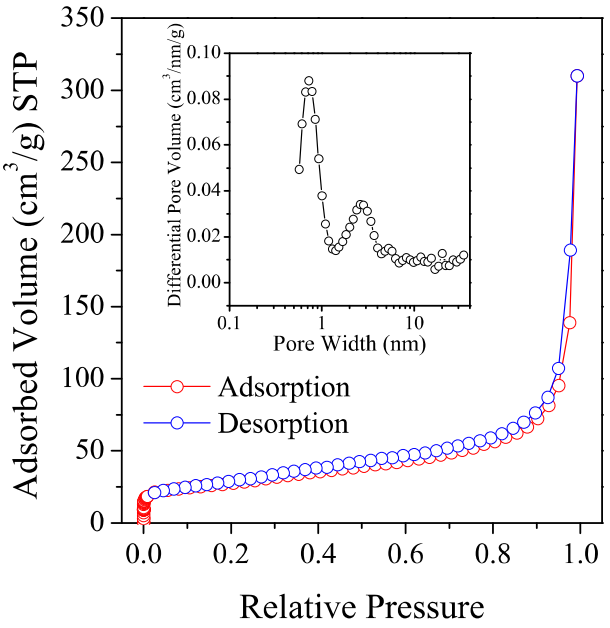

Figure 7. Adsorption-desorption isotherm of CNWs obtained using N_2 gas at 77 K. Inset shows the pore width distribution calculated by the quenched solid density functional theory (QSDFT) method [33].

4. Conclusions

The deposition of CNW film on a silicon substrate is demonstrated by the SWPECVD. The orientation of CNWs proximity to the substrate surface was horizontal and that at the top of the film is vertical. A CNW is composed of well-crystallized nanographite with a lateral and longitudinal sizes of approx. 10 and 5 nm, respectively. The deposition of CNW film, in particular, the film thickness strongly depends on the methane concentration, deposition pressure, distance between substrate and quartz disk, and deposition duration. The deposition rate in terms of the film thickness is approx. 1 μm/min. The strong dependence of the deposition pressure and distance between substrate and quartz disk on the film thickness and domain size revealed that the charged particles play an important role in the growth of CNWs. The growth of CNWs can be described as continuous processes of nucleation and growth of nanographite crystallites, which is consistent with the thermodynamic model of nucleation. The nitrogen gas adsorption measurements show that the CNW film has approx. 100 m^2/g BET specific surface area with micro-mesopores.

Acknowledgements

Part of this study has been supported by a Grant for the Strategic Development of Advanced Science and Technology S1101017 organized by the Ministry of Education, Culture, Sports, Science and Technology (MEXT) since April 2011. Authors would like to thank Mr. K. Hirakawa, and Mr. K. Yanagisawa for their technical support in TEM measurement. Authors are also grateful to Rigaku Corporation for XRD measurement.

Notes and references

[a] *Graduate School of Interdisciplinary New Science, Toyo University, 2100 Kujirai, Kawagoe-shi, Saitama 350-8585, Japan. E-mail: uchida_t@toyo.jp*

[b] *Bio-Nano Electronics Research Centre, Toyo University, 2100 Kujirai, Kawagoe-shi, Saitama 350-8585, Japan.*

[c] *Graduate School of Science and Engineering, Toyo University, 2100 Kujirai, Kawagoe-shi, Saitama 350-8585, Japan.*

† Present address: Device Functional Analysis Department, NISSAN ARC, Ltd., 1, Natsushima-cho, Yokosuka, Kanagawa 237-0061, Japan.

1. A. K. Geim, *Science*, 2009, **324**, 1530-1534.
2. P. J. F. Harris, *Carbon Nanotube Science, Synthesis, Properties and Applications*, Cambridge University Press, 2009.
3. Y. H. Wu, P. W. Qiao, T. C. Chong and Z. X. Shen, *Advanced Materials*, 2002, **14**, 64-67.
4. K. Kobayashi, M. Tanimura, H. Nakai, A. Yoshimura, H. Yoshimura, K. Kojima and M. Tachibana, *Journal of Applied Physics*, 2007, **101** 094306.
5. M. Hiramatsu and M. Hori, *Carbon Nanowalls: Synthesis and Emerging Applications*, Springer-Verlag, 2010.
6. O. Tanaike, N. Kitada, H. Yoshimura, H. Hatori, K. Kojima and M. Tachibana, *Solid State Ionics*, 2009, **180**, 381-385.
7. E. C. Stancu, M. D. Ionita, S. Vizireanu, A. M. Stanciuc, L. Moldovan and G. Dinescu, *Materials Science and Engineering B-Advanced Functional Solid-State Materials*, 2010, **169**, 119-122.
8. A. Achour, B. E. Belkerk, K. A. Aissa, S. Vizireanu, E. Gautron, M. Carette, P. Y. Jouan, G. Dinescu, L. Le Brizoual, Y. Scudeller and M. A. Djouadi, *Applied Physics Letters*, 2013, **102** 061903.
9. S. C. Shin, A. Yoshimura, T. Matsuo, M. Mori, M. Tanimura, A. Ishihara, K.-i. Ota and M. Tachibana, *Journal of Applied Physics*, 2011, **110** 104308.
10. A. T. H. Chuang, B. O. Boskovic and J. Robertson, *Diamond and Related Materials*, 2006, **15**, 1103-1106.
11. A. T. H. Chuang, J. Robertson, B. O. Boskovic and K. K. K. Koziol, *Applied Physics Letters*, 2007, **90** 123107.
12. P. Hojati-Talemi and G. P. Simon, *Carbon*, 2010, **48**, 3993-4000.
13. K. Tanaka, M. Yoshimura, A. Okamoto and K. Ueda, *Japanese Journal of Applied Physics Part 1-Regular Papers Brief Communications & Review Papers*, 2005, **44**, 2074-2076.
14. Y. H. Wu, *Nano Letters*, 2002, **2**, 355-359.
15. M. Hiramatsu, K. Shiji, H. Amano and M. Hori, *Applied Physics Letters*, 2004, **84**, 4708-4710.
16. K. Shiji, M. Hiramatsu, A. Enomoto, N. Nakamura, H. Amano and M. Hori, *Diamond and Related Materials*, 2005, **14**, 831-834.
17. S. Vizireanu, L. Nistor, M. Haupt, V. Katzenmaier, C. Oehr and G. Dinescu, *Plasma Processes and Polymers*, 2008, **5**, 263-268.
18. H. G. Jain, H. Karacuban, D. Krix, H.-W. Becker, H. Nienhaus and V. Buck, *Carbon*, 2011, **49**, 4987-4995.
19. S. Kurita, A. Yoshimura, H. Kawamoto, T. Uchida, K. Kojima, M. Tachibana, P. Molina-Morales and H. Nakai, *Journal of Applied Physics*, 2005, **97**, 5.
20. T. Mori, M. Hiramatsu, K. Yamakawa, K. Takeda and M. Hori, *Diamond and Related Materials*, 2008, **17**, 1513-1517.
21. G. Sato, T. Morio, T. Kato and R. Hatakeyama, *Japanese Journal of Applied Physics Part 1-Regular Papers Brief Communications & Review Papers*, 2006, **45**, 5210-5212.
22. N. G. Shang, F. C. K. Au, X. M. Meng, C. S. Lee, I. Bello and S. T. Lee, *Chemical Physics Letters*, 2002, **358**, 187-191.
23. Z. Bo, Y. Yang, J. H. Chen, K. H. Yu, J. H. Yan and K. F. Cen, *Nanoscale*, 2013, **5**, 5180-5204.
24. T. Kimura, Y. Yoshida and S. I. Mizuguchi, *Japanese Journal of Applied Physics, Part 2 (Letters)*, 1995, **34**, L1076-L1078.
25. L. G. Cancado, K. Takai, T. Enoki, M. Endo, Y. A. Kim, H. Mizusaki, A. Jorio, L. N. Coelho, R. Magalhaes-Paniago and M. A. Pimenta, *Applied Physics Letters*, 2006, **88**, 3.
26. N. Jiang, H. X. Wang, H. Zhang, H. Sasaoka and K. Nishimura, *Journal of Materials Chemistry*, 2010, **20**, 5070-5073.
27. H. Yoshimura, S. Yamada, A. Yoshimura, I. Hirosawa, K. Kojima and M. Tachibana, *Chemical Physics Letters*, 2009, **482**, 125-128.
28. C. Gomez-Aleixandre, O. Sanchez, A. Castro and J. M. Albella, *Journal of Applied Physics*, 1993, **74**, 3752-3757.
29. K. Teii, S. Shimada, M. Nakashima and A. T. H. Chuang, *Journal of Applied Physics*, 2009, **106**, 6.
30. J. Thomson, Joseph, *Conduction of Electricity through Gases*, second edithon edn., Cambrige University press, 1906.
31. S. Yugo, T. Kanai, T. Kimura and T. Muto, *Applied Physics Letters*, 1991, **58**, 1036-1038.
32. Y. Lifshitz, T. Kohler, T. Frauenheim, I. Guzmann, A. Hoffman, R. Q. Zhang, X. T. Zhou and S. T. Lee, *Science*, 2002, **297**, 1531-1533.
33. A. V. Neimark, Y. Z. Lin, P. I. Ravikovitch and M. Thommes, *Carbon*, 2009, **47**, 1617-1628.

High deposition rate, control of domain size, detailed characterization and charged particle-induced growth mechanism of CNW films are reported.